Available online at www.sciencedirect.com
SCIENCE DIRECT®
Vision Research 45 (2005) 1047–1062
Vision Research
www.elsevier.com/locate/visres

Contour curvature polarity and surface interpolation

C. Fantoni [a,c,*], M. Bertamini [b,1], W. Gerbino [c,2]

[a] Department of Sciences of Languages, University of Sassari, via Roma 14, 74100 Sassari, Italy
[b] School of Psychology, University of Liverpool, Bedford Street South, L69 7ZA Liverpool, UK
[c] Department of Psychology and B.R.A.I.N. Centre for Neuroscience, University of Trieste, via Sant'Anastasio 12, 34134 Trieste, Italy

Received 24 April 2004; received in revised form 8 October 2004

Abstract

Contour curvature polarity (i.e., concavity/convexity) is recognized as an important factor in shape perception. However, current interpolation models do not consider it among the factors that modulate the trajectory of amodally-completed contours. Two hypotheses generate opposite predictions about the effect of contour polarity on surface interpolation. *Convexity advantage*: if convexities are preferred over concavities, contours of convex portions should be more extrapolated than those of concave portions. *Minimal area:* if the area of amodally-completed surfaces tends to be minimized, contours of convex portions should be less extrapolated than contours of concave portions. We ran three experiments using two methods, simultaneous length comparison and probe localization, and different displays (pictures vs. random dot stereograms). Results indicate that contour polarity affects the amodally-completed angles of regular and irregular surfaces. As predicted by the minimal area hypothesis, image contours are less extrapolated when the amodal portion is convex rather than concave. The field model of interpolation [Fantoni, C., & Gerbino, W. (2003). Contour interpolation by vector-field combination. *Journal of Vision, 3*, 281–303. Available from http://journalofvision.org/3/4/4/] has been revised to take into account surface-level factors and to explain area minimization as an effect of surface support ratio.

Keywords: Amodal completion; Interpolation; Convexity; Good continuation; Random dot stereograms

Both local and global factors are known to affect amodal completion (Boselie & Leeuwenberg, 1986; Kanizsa, 1979; Kellman & Loukides, 1987; Kellman & Shipley, 1991; Leeuwenberg, 1982; Sekuler, 1994). In this paper we analyze contour curvature polarity (CCP), which is the spatial property of a surface boundary of being either convex or concave, and show its effect on amodally-completed portions of partially-occluded surfaces. This is a surface-level factor, more global than contour-level factors like good continuation, but less global than factors like symmetry that has been shown to affect amodal completion (Gerbino, Sgorbissa, & Fantoni, 2000; van Lier, van der Helm, & Leeuwenberg, 1994; van Lier & Wagemans, 1999). The CCP effects reported here suggest that visual interpolation is sensitive to the minimization of surface area, independent of its specific shape.

1. What is contour curvature polarity?

There has been great interest in CCP recently (Barenholtz, Cohen, Feldman, & Singh, 2003; Bertamini, 2001; Bertamini & Croucher, 2003; Hulleman, te Winkel, & Boselie, 2000; Singh & Hoffman, 2001; Xu & Singh, 2002), also because this image feature is informative

* Corresponding author. Tel.: +39 0405582766; fax: +39 0404528022.
E-mail addresses: fantoni@psico.units.it (C. Fantoni), m.bertamini@liverpool.ac.uk (M. Bertamini), gerbino@units.it (W. Gerbino).
[1] Tel.: +4401517942954; fax: +4401517942945.
[2] Fax: +390404528022.

0042-6989/$ - see front matter © 2004 Elsevier Ltd. All rights reserved.
doi:10.1016/j.visres.2004.10.023

about solid shape (Hoffman & Richards, 1984; Koenderink, 1984). To achieve a formal definition of CCP we should consider together the notions of curvature polarity and contour ownership.

As depicted in Fig. 1, *curvature polarity* is defined here with reference to a smooth 2D line containing an inflection point. The line acts as a bilateral contour for two adjacent portions of the plane. The region that includes all chords connecting any pair of points on the contour is locally convex (+); while the complementary region is concave (−). Within the same portion of the plane, a concave region blends into a convex region in the neighborhood of the inflection point.

This paper is concerned with curvature polarity; i.e., with the sign of curvature. However, let us mention some related concepts. Another local measure is the *magnitude of curvature*, conveniently described by the change of orientation of a tangent sliding along the contour (Feldman & Singh, 2005). Minima and maxima of curvature (Attneave, 1954; Norman, Phillips, & Ross, 2001) as well as inflections (i.e., inversions of curvature polarity) provide the building blocks of the *curvature primal sketch*, the early representation proposed by Asada and Brady (1984). More global measures of *shape convexity* apply to closed contours (i.e., generic polygons). Different synthetic measures of closed-contour curvature can be considered. A perimeter-based measure of shape convexity can be derived from curvature polarity, by computing the proportion of locally-convex contour lengths over the total contour length. A surface-based measure of shape convexity is the proportion of the area of the polygon, over its convex hull (Preparata & Shamos, 1985; Zunic & Rosin, 2002). Both measures range between an asymptotic 0 and 1; where values close to 0 represent star figures with long figural rays and large concavities, while 1 stands for strictly convex surfaces like a circle. According to this approach closed contours define shapes that can be either totally or partially convex.

Curvature polarity is conveniently labeled by marking the convex region with a plus sign and the concave region with a minus sign. The +/− labeling for convex/concave seems appropriate because, other things being equal, the convex region tends to be perceived as the figure and the concave region as the ground (Koffka, 1935 [p. 192]; Rubin, 1921).

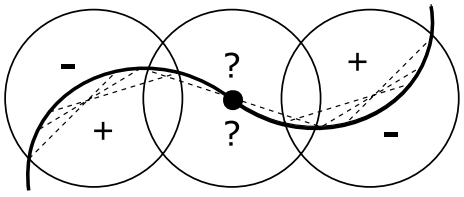

Fig. 1. Change of curvature polarity along a smooth contour with an inflection (black dot). Dashed lines are chords. The contour segment within an aperture (circle) locally defines two regions. If the contour within the aperture has no inflections, the region including all chords between any pair of points on the contour is convex (+) and the other concave (−). If the contour within the aperture brackets an inflection, chords intersect the contour and curvature polarity is locally ambiguous.

The assignment of figure/ground (F/G) roles to adjacent regions bounded by closed contours depends on various factors. Following Arnheim (1954), Kanizsa and Gerbino (1976) put convexity against symmetry and relative area, and demonstrated the strength of convexity as a disambiguating factor in F/G assignment. Recent computer vision research (Baek & Sajda, 2003; Pao, Geiger, & Rubin, 1999) provided consistent conclusions. However, convexity can be overcome and ground regions bounded by (totally or partially) convex contours can be perceived, like in holes.

The perceptual process of F/G assignment defines *contour ownership* (Koffka, 1935). The contour that geometrically separates two adjacent regions perceptually belongs to the figure only; that is, the contour tends to be perceived as an occluding edge which bounds a surface but not the ground behind it. Contour ownership plays a crucial role in various psychophysical tasks (Baylis & Driver, 2001; Bertamini, Friedenberg, & Argyle, 2002; Nakayama, Shimojo, & Silverman, 1989).

The combination of curvature polarity and contour ownership generates the notion of contour curvature polarity (CCP). Following Feldman and Singh (2005) among others, we will label figural contours as *positive* when convex and *negative* when concave. Wholly-convex surfaces (triangles, squares, disks) are bounded by positive contours only. Partially-convex surfaces are bounded by both positive and negative contours. Note that partially-convex surfaces are often called concave, just because they are not wholly convex (Massironi, 2002).

Apparently contrasting CCP effects have been reported. A peculiar visual search asymmetry involves the concavity/convexity dichotomy; a target with a concavity among convex distractors is more easily detected than a convex target among distractors with concavities (Hulleman et al., 2000; Humphreys & Müller, 2000). A similar effect was found by Barenholtz et al. (2003) in change detection; observers are more accurate when the shape change consists in the introduction or removal of a concavity, compared to a convexity. Different CCP effects support the notion of a convexity advantage for the discrimination of the relative position of two angles (Bertamini, 2001; Bertamini & Croucher, 2003; Bertamini & Mosca, 2004; Gibson, 1994).

As suggested by Bertamini (2001) a common explanation for such effects could be grounded on the minima rule (Hoffman & Richards, 1984; Xu & Singh, 2002); i.e., on the assumption that concavities mark the articulation of a whole into parts, while convexities belong to component parts. This would explain why observers are

better in detecting concavities, although they may be imprecise in judging their spatial position.

2. Contour polarity and visual interpolation

More relevant for the present study, Liu, Jacobs, and Basri (1999) provided an indirect demonstration that CCP affects interpolation processes. Observers should discriminate whether two regions grouped into an amodally-completed form were coplanar or not. Liu et al. (1999) assumed that the stronger the grouping between the two regions, the harder it will be to resolve their relative stereoscopic depth. They predicted and found that stereoacuity was lower for convex forms.

Such a finding is consistent with a classification of connectable regions proposed by Jacobs (1996) and Liu et al. (1999). Consider the connection between two convex regions defined by the rectilinear extrapolations of two pairs of T-stems (Fig. 2). Each region may include or not the opposite pair of endpoints. Four types of relationships are distinguishable:

Type I: each region includes the opposite pair of endpoints;
Type I.5: one region, but not the other, includes the opposite pair of endpoints;
Type II: the two regions overlap but neither includes the opposite pair of endpoints;
Type III: the two regions do not overlap.

According to Jacobs (1996) and Liu et al. (1999) the strength of region grouping follows the above ordering. Notice that only *type I* regions can be grouped into a convex amodally-completed form. Parts of a convex partially-occluded surface would be more strongly connected than parts of any surface with an amodal concavity.

In this paper we evaluate the role of CCP in visual interpolation by studying the amodal completion of partially-occluded *explementary* angles (i.e., angles that add up to 360 degrees: http://thesaurus.maths.org). The shape of interpolated figural contours bounding an occluded convex angle is contrasted with the shape of interpolated figural contours bounding an occluded explementary (concave) angle. Any contour-level theory would predict the same interpolation for both angles. We report an effect of CCP on the shape of interpolation trajectories and attribute it to surface completion processes.

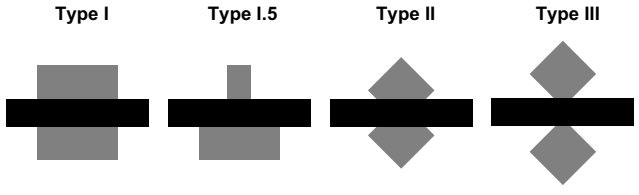

Fig. 2. Four types of relationships between convex regions (Jacobs, 1996; Liu et al., 1999).

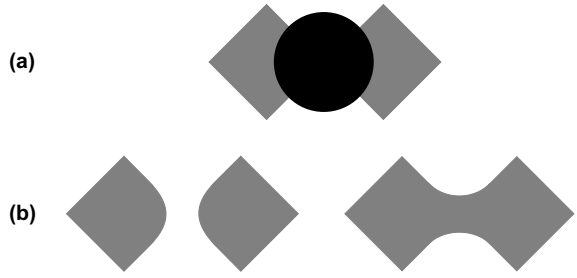

Fig. 3. (a) A configuration in which the grouping of contour fragments is geometrically balanced. (b) The two solutions are equivalent at the contour level, but differ with respect to CCP and object numerosity. Naive observers tend to prefer the convex solution on the left.

Another important question about amodal completion is how the correspondence problem is solved (i.e., which contour fragments are grouped together when they are more than two). Takeichi, Nakazawa, Murakami, and Shimojo (1995) formalized the correspondence problem, but did not consider CCP as a possible determining factor. Fig. 3 suggests that CCP can disambiguate the correspondence between fragments (Gerbino & Fantoni, 2002). Left and right solutions in Fig. 3(b) are equivalent at the contour-level, given that the four endpoints are equidistant. However, when asked to describe Fig. 3(a), 10 observers out of 10 reported seeing two convex diamonds instead of a single concave hourglass shape. In this case convexity wins over object numerosity.

In this paper, rather than studying the disambiguating role of CCP, we focused on the perceived shape of the interpolated contour. In Experiments 1 and 3 a display similar to Fig. 3(a) was used. However, the separation between T-junctions was increased to make the amodal completion of a concave partially-occluded object even less likely.

3. Contour-level and surface-level factors

Most empirical work on visual interpolation has focused on how interpolation is affected by contour-level factors such as position and orientation of T-stems (Fantoni & Gerbino, 2002; Gerbino & Fantoni, 2000; Kellman & Shipley, 1991). Fantoni and Gerbino (2003) modeled interpolated trajectories as a compromise between good continuation (GC) of contour fragments and minimal path (MP) between endpoints. Support ratio has been considered at the level of contours (Shipley & Kellman, 1992) and surfaces (Gerbino & Fantoni, 2000). However, the role of CCP, which is a surface-level factor, has not been investigated until now.

Consider Fig. 4(a). Contour-based interpolation models (Guy & Medioni, 1996; Mumford, 1994; Ullman, 1976; Williams & Jacobs, 1997; for a review see Fantoni & Gerbino, 2003) would predict that the perceived separation between vertices of the two occluded angles is the same in both cases (hourglass vs. diamonds), given that positions and orientations of the four T-stems are the same. On the contrary, a difference in vertex separation would be consistent with surface-based interpolation processes, given that the two configurations are unbalanced at the surface level. Let us contrast two hypotheses (convexity advantage vs. minimal area) predicting opposite deviations from the default trajectory determined only by contour-based factors.

Convexity advantage. The convexity advantage observed in figure/ground organization (Kanizsa & Gerbino, 1976) can be explained by a tendency to avoid or minimize the perception of concave figures. A related effect might occur in visual interpolation. The visual system would minimize the (negative) curvature of the interpolated contour required to perceive a smooth concavity. The field model by Fantoni and Gerbino (2003) could account for a convexity advantage by assuming that GC is stronger (i.e., T-stems are more extrapolated) in the convex case, relative to the concave case. The interpolation trajectory would penetrate more into the occluded space when the angle is convex rather than concave. In Fig. 4(b), occluded vertices of the concave hourglass should appear more separated than vertices of the two convex diamonds. This possible effect would be related to the convexity advantage for the discrimination of relative positions of angles (Bertamini, 2001; Bertamini & Croucher, 2003; Gibson, 1994).

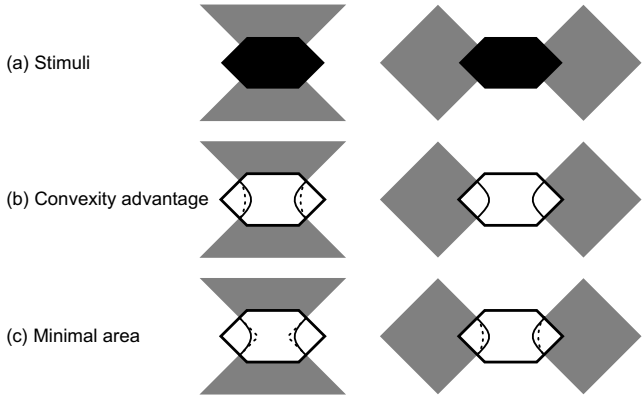

Fig. 4. (a) At the contour level, the hourglass polygon on the left and the two diamond shapes on the right should be amodally completed along the same trajectories. However, occluded concavities of the hourglass polygon appear closer than occluded convexities of the two diamonds. Opposite predictions are generated by different hypotheses. (b) The convexity advantage hypothesis predicts a larger perceived separation between concave angles. (c) The minimal area hypothesis predicts the opposite. Continuous lines represent default trajectories based on contour-level factors (GC and MP). Dotted lines show trajectories biased towards either GC or MP.

Minimal area. If perception is affected by the cost of representing object surfaces, interpolated contour trajectories should be affected by the tendency to minimize the area of partially-occluded surfaces. In terms of the field model by Fantoni and Gerbino (2003), the interpolated contour of a convex angle would be closer to MP than the interpolated contour of the explementary concave angle. The tendency to area minimization would cooperate with MP (against GC) in the convex case, while it would cooperate with GC (against MP) in the concave case. In Fig. 4(c), occluded vertices of the concave hourglass should appear closer than vertices of the two convex diamonds.

The above-described contrast does not consider the possibility that the convexity advantage is so strong to support the perception of Fig. 4(a)-left as two partially-overlapping triangles behind a hexagon. Though unlikely (given that T-junction separations are much smaller along the vertical than along the horizontal) this possibility cannot be dismissed. It predicts effects in the same direction as the minimal area hypothesis in Experiments 1 and 3, in which observers matched a comparison line to the horizontal separation between occluded intersections of T-stem extrapolations in configurations like Fig. 4(a). However, it does not apply to Experiment 2, where evidence consistent with the minimal area hypothesis was obtained using configurations different from Fig. 4(a).

Note that the minimal area hypothesis predicts different interpolation trajectories when the same surrounded region is perceived as a hole, rather than a solid figure. If the minimization refers to the material surface, as specified in the above definition, the interpolated contour will be closer to MP when the surrounded region is perceived as a figure in front of the background, than when it is perceived as a hole. This prediction is tested in Experiment 3.

4. Summary of experiments

In Experiment 1 we measured the perceived separation of occluded vertices in configurations of the type shown in Fig. 4. Observers were required to compare the length of a line with the horizontal separation between two vertices. The critical contrast was between convex or concave angles. The simultaneous length comparison allowed us to obtain a quantitative estimate of perceived separation.

In Experiment 2 we probed the shape of amodally-completed angles belonging to regular or irregular surfaces. Observers judged if a probe briefly flashed on the occluded region was inside or outside the amodally-completed angle. Again the critical comparison

was between convex and concave angles, but unlike in Experiment 1 only one angle was partially occluded. This allowed us to validate the minimal area hypothesis against the possibility that patterns like the one in Fig. 4(a)-left are perceived as two partially-overlapping triangles. Moreover, to insure that our findings were not entirely due to a difference in size or perceived regularity between conditions we also tested symmetric vs. asymmetric shapes having the same area.

In Experiment 3 we used an adjustment task to measure the perceived separation between amodally-completed angles similar to those of Experiment 1. To manipulate CCP we introduced random dot stereograms. In the crossed-disparity condition the surrounded region was perceived as a solid surface with concave partially-occluded angles; while in the uncrossed-disparity condition the surrounded region was perceived as a hole and observers evaluated the separation between vertices of the explementary (convex) partially-occluded angles, belonging to the surrounding surface. The advantage of this methodology is that the same region is turned from a plenum to a vacuum by changing the disparity from crossed to uncrossed (Bertamini & Mosca, 2004).

Let us anticipate our findings. Contour-level factors alone do not explain visual interpolation. CCP is a surface-level factor affecting the shape of interpolated trajectories in the direction predicted by the minimization of surface area. In the final discussion the field model of interpolation (Fantoni & Gerbino, 2003) has been revised to take into account surface-level factors and to explain area minimization as an effect of surface support ratio.

5. Experiment 1: Simultaneous length comparison

To evaluate the effect of CCP on interpolated trajectories (i.e., the difference in amodally completing convex vs. concave angles), we measured the perceived separation between two horizontally-aligned occluded vertices belonging to convex or concave angles. Since the difference between open and closed spaces represents a possible confound, we ran baseline conditions with non-occluded angles. Hence, the experiment included two factors, relative to properties of target angles: CCP (concave vs. convex) and occlusion (non-occluded vs. occluded), factorially combined in a 2×2 between-subjects design (Fig. 5(a)).

There are reasons to expect a CCP effect also in the baseline non-occluded condition. According to the minimal area hypothesis, material surfaces (i.e., figures) should appear smaller than empty inter-figural spaces also when they are fully specified in the stimulus image. However, a substantial increment of this difference is expected if minimal area acts as a factor in surface interpolation.

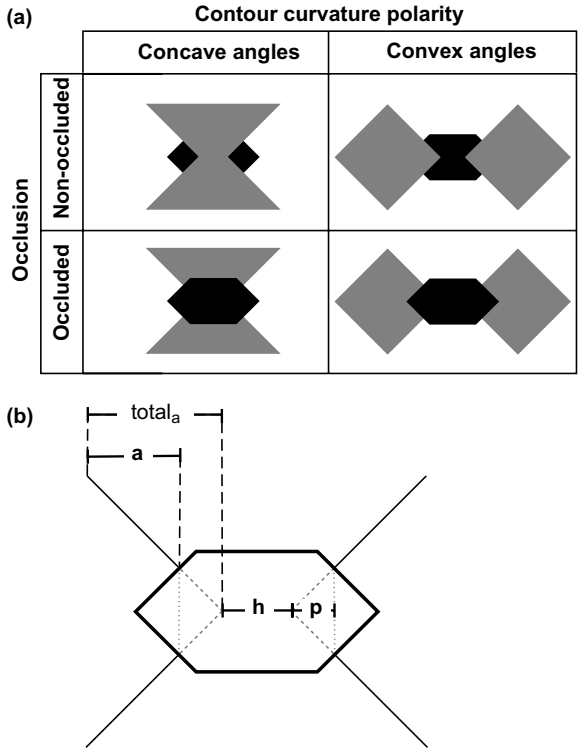

Fig. 5. (a) The four conditions of Experiment 1. (b) Symbols used to refer to main stimulus parameters.

6. Method

6.1. Participants

Thirty-six undergraduate students of the University of Trieste, with normal or corrected-to-normal vision, served as unpaid participants in a 10-min individual session. They were familiar with amodal completion phenomena, but naive to the purpose of the experiment. Participants were randomly assigned to one of the four experimental conditions.

6.2. Apparatus and displays

Stimuli were displayed in a dark room on a computer monitor (LG StudioWorks 775E), set at the 1024×768 pixel resolution. Observers were seated at a distance of 58 cm from the screen. Three luminance levels were used: high (90 cd/m^2) for the white background; intermediate (29 cd/m^2) for regions perceived as grey partially-occluded shapes; low (3 cd/m^2) for the region perceived as a black hexagon.

The non-occluded condition was used as a baseline to test for possible tendencies unrelated to amodal completion (i.e., minimization of background area and object numerosity).

The hourglass polygon including concave angles covered an overall HV extent of 202×162 pixels and was

either behind (occluded condition) or before (non-occluded condition) a central black hexagon. Convex configurations covered an overall HV extent of 364×162 pixels and included two diamonds (45°-rotated squares) with a 162-pixel diagonal. Also in convex conditions diamonds were either behind or before the central black hexagon.

As shown in Fig. 5(b) the four configurations shared the following features: (i) orthogonal T-junctions; (ii) length of the minimal path between line endings, MP-line length = 50 pixels; (iii) distance between MP-line and GC-vertex (junction of rectilinear extrapolations of T-stems), $p = 25$ pixels; (iv) horizontal separation between vertices, $h = 40$ pixels; (v) contour support ratio $a/\text{total}_a = 0.7$, taking the partially-occluded side as the reference length.

A grey two-pixel-thick horizontal line (29 cd/m^2) was randomly displayed on the left or right of each display. The amount of eccentricity between the center of the line and the center of the screen was 6.8°. The configuration and the line were shown simultaneously. In each trial the line length was randomly selected amongst 8 different values (10, 19, 27, 36, 44, 53, 61, 70 pixels).

6.3. Procedure

Participants were seated in front of the monitor with their head comfortably supported by a chin rest. They were tested individually in an experimental session introduced by instructions and training. The experimenter illustrated the configurations using printed displays and explained that similar patterns would be shown on a monitor during the experiment. Viewing was binocular.

Observers' ability to provide length estimates was tested in a brief preliminary session. Observers of the non-occluded condition estimated the horizontal separation between two angles (either convex or concave, depending on the group). Observers of the occluded condition draw the target shapes (grey surfaces in the lower row of Fig. 5) as they appeared to them behind the occluder and evaluated the vertex separation. Drawings demonstrated that occluded angles were perceived as horizontally separated. Observers in the occluded/convex group drew two separate diamonds, while those in the occluded/concave group drew a single concave polygon. All observers were able to provide reasonable numerical estimates of the vertex separation both with and without occlusion.

Next, observers were trained on the simultaneous length-matching task by completing a practice session of 4 trials, randomly extracted from the set of possible trials. In each trial they should judge whether the horizontal separation between the two vertices was *shorter* or *longer* than the length of the comparison line. Two keys were used to code responses. Observers were instructed to respond as quickly and accurately as possible.

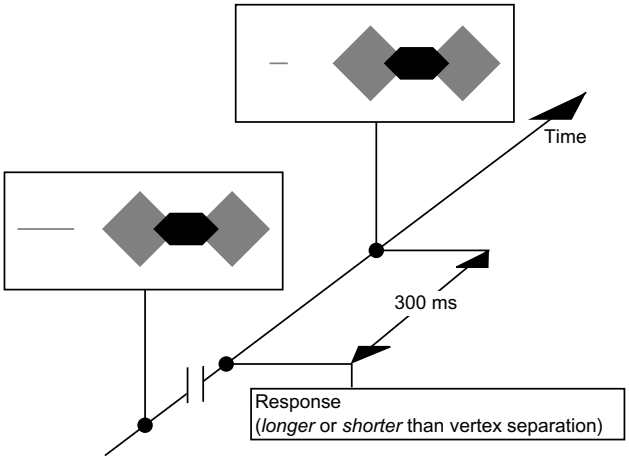

Fig. 6. Temporal sequence illustrating two successive trials of Experiment 1. These trials refer to condition in which the simultaneous length-matching task consisted in judging whether the horizontal line was perceived as longer or shorter than the separation between occluded vertices of the grey diamonds.

The experimental session included the random presentation of 64 trials (8 comparisons × 8 repetitions). Any simultaneous length-matching trial included three stages: (i) stimulus presentation; (ii) observer's response and stimulus termination; (iii) 300-ms blank interval before the presentation of the successive trial (Fig. 6).

7. Results

We analyzed the distribution of *estimated* vertex separations in different conditions. A 40-pixel estimate would match h, the *objective* horizontal separation which in occluded conditions was defined as the distance between junctions of the rectilinear extrapolations of T-stems.

Estimated vertex separations, for every observer, were calculated by probit analysis (Finney, 1962; Guilford, 1963). Proportions of "comparison line *longer* than vertex separation" responses were plotted as a function of line length (ranging from 10 to 70 pixels). The two tails of the individual probability distributions were eliminated and the three central values were transformed using the inverse of the cumulative normal. Then, the best-fitting straight line through the remaining points was computed to identify the x-value corresponding to its intersection with the $y = 0$ line. Such x-values (in pixel units) were the individual estimates of vertex separation.

Fig. 7(a) shows means and sem of estimated vertex separations for the 4 groups of 8 observers. Means are plotted relative to objective separation (40 pixels). As expected, the pattern of mean vertex separations is

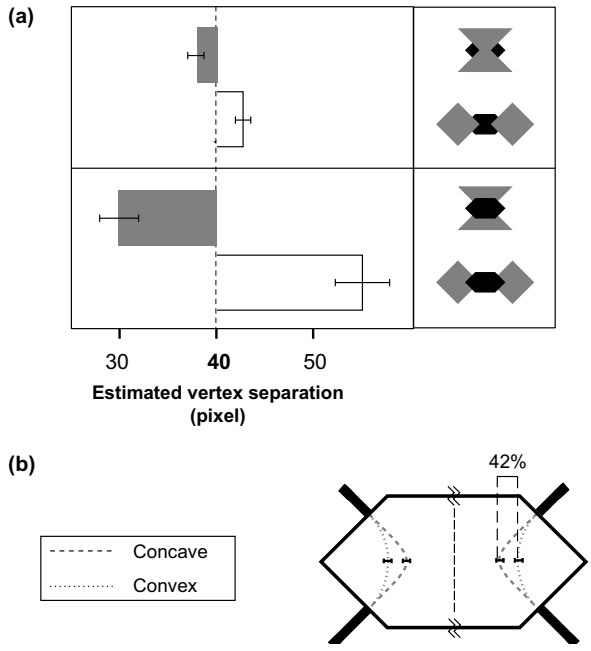

Fig. 7. (a) Mean estimated vertex separations and standard errors of the mean (error bars = ±1 sem) as a function of CCP and occlusion. (b) Visualization of the CCP effect on interpolated trajectories. Estimated separations in the non-occluded condition were discounted to evaluate the component effect attributable to surface-based interpolation processes. The differential penetration of interpolation trajectories amounts to 42% of the distance between the MP-line (0%) and the GC-vertex (100%).

consistent with a CCP effect for both occluded and non-occluded surfaces, as well as with a larger effect for occluded (concave = 29.2 pixels; convex = 55.0 pixels) than non-occluded (concave = 37.9 pixels; convex = 42.7 pixels) surfaces.

Statistical tests were performed after transforming raw data in the following way. Underestimations and overestimations of vertex separations were converted into relative contrast percentages [$M = 100\ (x - 40)/(x + 40)$]. Then, to equalize the variances of the four distributions the signed square root of M was taken as the transformed score. Resulting means and sem were as follows: concave/non-occluded [-1.03 ± 0.52]; convex/non-occluded [1.47 ± 0.36]; concave/occluded [-3.79 ± 0.49]; convex/occluded [3.81 ± 0.31].

The analysis of variance confirmed the substantial increase of the CCP effect in the occluded condition, relative to the baseline non-occluded condition: the interaction between CCP and occlusion [$F(1,32) = 35.67$, $p < 0.001$] as well as the main effect of CCP [$F(1,32) = 138.83$, $p < 0.001$] were significant. Average estimates for convex vs. concave angles were symmetrically distributed across h, as suggested by the lack of any effect of occlusion [$F < 1$].

Interestingly, in the non-occluded condition the difference between the separations of concave vs. convex angles was small (2.5 pixels) but significant [$F(1,32) = 17.12$, $p < 0.001$], consistent with the general idea that figures are perceived as smaller than inter-figural spaces.

If the baseline errors are discounted, the best estimates of CCP effects on the amodal completion of partially-occluded angles are 31.4 and 52.3 pixels for concave and convex conditions. Planned one-tailed t-tests against the value of 40 confirmed that both the underestimation of concave-angle separation [$t(17) = -4.3$, $p < 0.001$] and the overestimation of convex-angle separation [$t(17) = 4.4$, $p < 0.001$] were significant.

We suggest that the underestimation and overestimation of occluded vertex separations (for concave and convex angles, respectively) reflect different amounts of penetration of interpolated trajectories (IT) into the region defined by the MP-line and the GC-lines. An IT penetration of 0% would correspond to an interpolation along the MP-line, while an IT penetration of 100% would correspond to a sharp corner along GC-lines. Fig. 7(b) provides a visualization of the CCP effect estimated from data obtained in Experiment 1. When angles are occluded, the differential IT penetration attributable to CCP amounts to 42%, corresponding to 10.5 pixels (half of the difference between underestimated and overestimated separations) out of 25 pixels (p, the distance between the MP-line and the GC-vertex).

8. Discussion

Experiment 1 indicates that CCP affects the interpolation of T-stems. The amodal penetration into the interpolation triangle defined by GC- and MP-lines is smaller for convex angles than for explementary concave angles. The differential IT penetration amounts to 42% of the total distance between the GC-vertex and MP.

Contour-level processes alone cannot explain such an effect. Any model of visual interpolation should include surface-level processes. The pattern of results obtained in Experiment 1 is at odds with the convexity advantage hypothesis, as described in the introduction. In general, results are consistent with the minimal area hypothesis, which can explain the significant though small CCP effect on the perceived separation of non-occluded angles (baseline condition), as well as the large effect found when angles are occluded.

8.1. Experiment 2: Probe localization

In Experiment 1 we found a substantial effect of CCP on the interpolation of partially-occluded angles, after discounting the effect for non-occluded stimuli. However, shape, numerosity, and area, different in concave and convex conditions (hourglass vs. diamonds), might constitute possible confounds. Furthermore, the

occluded/concave display of Experiment 1 was ambiguous, with respect to amodal completion, being compatible with two partially-overlapping triangles, as well as an hourglass.

To overcome such limitations, in Experiment 2 we used a probe localization task, that provides a more direct measure of amodally completed trajectories (Gerbino & Fantoni, 2000; Guttman & Kellman, 2004; Takeichi, 1995). Stimuli were modified to make amodal completion unambiguous, by occluding only one angle of a target surface specified by a single region. Symmetry of target surfaces was also manipulated.

Two experimental factors, CCP (convex vs. concave) and shape (symmetric vs. asymmetric), were combined in a 2×2 design (Fig. 8(a)). As regards CCP, the interpolation of convex angles was contrasted with the interpolation of explementary concave angles. The minimal area hypothesis predicts that vertex localization is biased towards the MP-line for convex angles and towards the GC-vertex for concave angles. The convexity advantage hypothesis makes the opposite prediction. As regards the main effect of shape, the GC-vertex should be localized more accurately in symmetric cases, given that completions maximizing symmetry (along horizontal and vertical axes) coincide with those in which T-stems are rectilinearly extrapolated. As regards a possible interaction between CCP and shape, the difference in IT penetration for concave vs. convex symmetric surfaces should be equally large to the one for asymmetric surfaces or smaller (because of a ceiling effect at high IT penetration values), but not larger.

Since it was practically impossible to keep areas of target surfaces constant over all conditions without affecting the structure of shapes, we kept the areas of the two asymmetric targets equal and introduced a large difference between areas of the two symmetric targets. This arrangement allowed us to consider asymmetric conditions as a baseline and attribute possible deviations obtained in symmetric conditions to differences in surface areas.

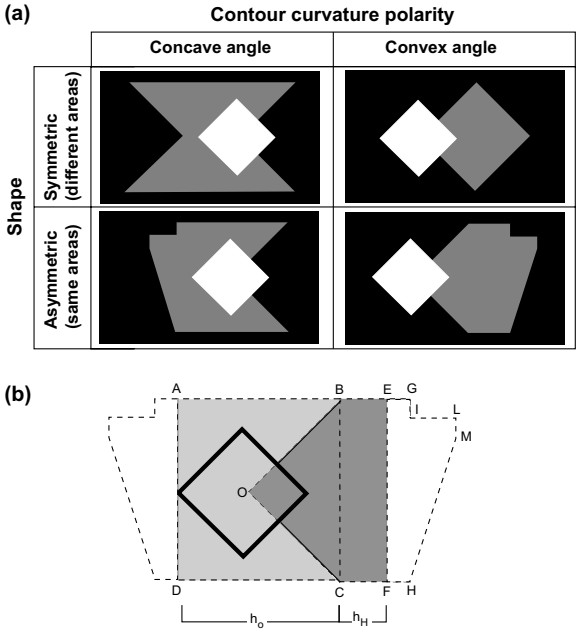

Fig. 8. (a) Displays used in Experiment 2. Labels refer to grey partially-occluded forms: rows for the shape factor and columns for the CCP factor. (b) Construction of asymmetric partially-occluded forms with the same area. The BCFE rectangle was adjusted to equalize the areas of BOCFE and BOCDA polygons. The asymmetric form with a convex occluded angle was obtained by joining BOCFE and EFHMLIG polygons; the one with a concave occluded angle by joining the BOCDA polygon and the polygon derived from the reflection of EFHMLIG.

9. Method

9.1. Participants

Twelve undergraduate students of the University of Trieste served as unpaid participants in a 15-min individual session. All had normal or corrected-to-normal vision. They were familiar with amodal completion, but naive with respect to the purpose of the experiment. They participated in all conditions of the factorial within-subjects design.

9.2. Apparatus and displays

The apparatus and the viewing distance were the same as in Experiment 1. We used 4 displays, corresponding to conditions of the CCP (2) $\times$ shape (2) design. Each display included a grey surface perceived as partially occluded by a diamond (Fig. 8(a)). Geometrically, each display was a mosaic of three regions: a white diamond (90 cd/m^2), a concave grey polygon (29 cd/m^2) and a concave black field (3 cd/m^2). The largest target surface (concave/symmetric grey polygon) covered an overall HV extent of 311×205 pixels. Constant features of all displays were as follows: contour support ratio = 0.7; white diamond diagonal = 142 pixels; MP-line length = 64 pixels; distance between GC-vertex and MP-line = 32 pixels.

The experiment was run in a dark room without dark adaptation. No fixation point was provided. The vertex of the white diamond horizontally aligned with the occluded vertex of the grey polygon and adjacent to the grey region was located at the center of the screen.

Symmetric targets were similar to those of Experiment 1. The convex target surface was a grey diamond (diagonal = 205 pixels); while the concave target surface was a hourglass polygon with the same contour support ratio and an area twice the area of the grey diamond. Asymmetric targets had the same area (Fig. 8(b)), 1.5 times the one of the grey diamond.

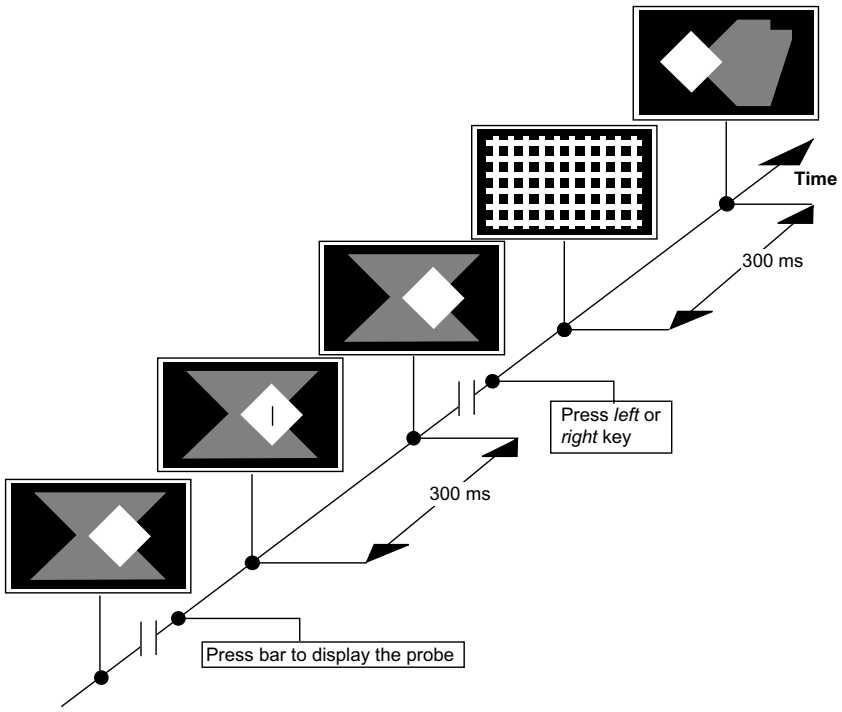

Fig. 9. Temporal sequence of a trial in Experiment 2. The probe localization task consisted in judging whether the briefly-presented probe appeared on the left/right of the perceived location of the occluded vertex.

To measure amodal contour trajectories, a red vertical probe (1×20 pixels) was randomly presented in one of 8 locations on the horizontal axis through the GC-vertex. The spatial range covered by probe locations was centered on the GC-vertex. Probe deviations from the MP-line were 54, 48, 42, 35, 29, 22, 16, 10 pixels. Such values corresponded to IT penetration values ranging from 169% (probe on the left of the GC-vertex) to 31% (probe on the left of the GC-vertex, close to the MP-line).

9.3. Design and procedure

Participants were seated in front of the monitor with their head comfortably supported by a chin rest. Viewing was binocular. The experimenter introduced amodal completion phenomena and the probe localization technique with the following words: ''This is an experiment on amodal completion of partially-occluded forms, the visual process that make us perceive contours as continuing behind occluding objects. In this experiment amodal completion is studied using patterns like the one on the monitor (one display of Fig. 8(a) was randomly selected). There will be many trials. In each trial, a vertical line will be shown briefly. You should judge if the line appears located on the *left* or *right* of the occluded vertex. Please focus your attention on the grey partially-occluded form and try to be as accurate as possible.''

After a training session of four trials randomly extracted from the set of 32 trial types (4 displays $\times$ 8 probe locations), participants completed the experimental session consisting of the random presentation of 256 trials (4 displays $\times$ 8 probe locations 8 repetitions).

As shown in Fig. 9, the probe localization technique included three steps: (i) the display was shown without the probe; (ii) when the observer felt that the amodal completion of the occluded angle was clear, he/she pressed the space bar to display the vertical probe for 300 ms; (iii) while the display without the probe was visible, the observer pressed a key or the left or right of the keyboard to judge whether the probe appeared on the left or right of the apparent location of the occluded vertex. After key press, a 300-ms mask was displayed and the next trial was presented.

10. Results

Following the probit procedure already used in Experiment 1, we computed the individual probe deviations corresponding to the 0.5 probability of ''left'' responses in each of the four conditions. Probe deviations in pixels were converted into per cent IT penetrations relative to the 32-pixel interval between the MP-line and the GC-vertex (Fig. 10(a)): a probe on the MP-line would correspond to an IT penetration of 0% and a probe on the GC-vertex to an IT penetration

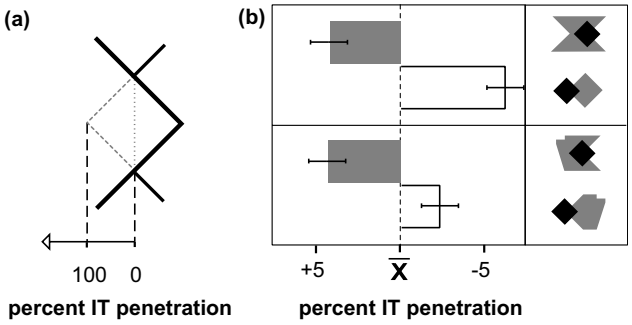

Fig. 10. (a) The IT penetration range between 0% (MP-line) and 100% (GC-vertex). (b) Mean deviations from the average IT penetration (x = 80.25%) and sem in the four conditions.

of 100%. Such a relative measure is convenient to compare data obtained in experiments with different displays.

Fig. 10(b) shows mean IT penetrations and sem in the four conditions, relative to the average value of 80.25%, taken as representative of the default trajectory based on contour-level factors alone.

Inspection of Fig. 10(b) indicates that the CCP effect found in Experiment 1 was replicated. IT penetration in concave conditions was higher than in convex conditions. However, contrary to expectations based on symmetry, the CCP effect was larger for symmetric surfaces. Results of a two-way repeated-measures analysis of variance confirm such observations. The main effect of CCP was significant: IT penetration was larger for concave (84.5%) than convex (76.0%) surfaces [$F(1,10) = 22.50$, $p < 0.001$]. The main effect of shape was not significant [$F(1,10) = 1.30$, $p = 0.27$]; notably, IT penetration was smaller for symmetric (79.2%) than asymmetric (81.3%) surfaces, opposite to symmetry-based predictions.

As regards the CCP × shape interaction, the CCP effect amounted to 6.6% for asymmetric surfaces (concave = 84.5% vs. convex = 77.9%) and 10.4% for symmetric surfaces (concave = 84.5% vs. convex = 74.1%), contrary to symmetry-based predictions. The increment of the CCP effect for symmetric surfaces, though statistically not significant [$F(1,10) = 3.00$, $p = 0.11$] run against the symmetry-based hypothesis, given that the CCP effect in the symmetric condition should be smaller or equal to the amount in the baseline (asymmetric) condition.

To account for the pattern of CCP effects in Fig. 10(b) we run a post-hoc analysis, using surface support ratio as a possible determinant of IT penetration. Surface support ratio was defined as the ratio between two areas, the one for the MP completion solution and the one for the GC completion solution. The difference between these two areas equals to the area on the interpolation triangle bounded by GC extrapolations and the MP-line. As the area of the interpolation region increases (relative to the total area of the partially occluded surface) the value of surface support ratio departs from 1 in opposite directions, decreasing for convex surfaces and increasing for concave surfaces. We computed surface support ratios for the 4 displays of Experiment 2, obtaining the following values: symmetric/concave = 1.024; symmetric/convex = 0.951; asymmetric/concave = 1.033; symmetric/convex = 0.967. A linear regression analysis showed that IT penetration positively correlated with surface support ratio for 10 out of 11 participants (with r values ranging from 0.46 to 0.99); for one participant the pattern of data was noisy ($r = -0.23$). On the average, surface support ratio explained 59% of the variance in individual data on vertex localization.

11. Discussion

By probing the location of partially-occluded vertices, in Experiment 2 we obtained a CCP effect consistent with the minimal area hypothesis. The IT penetration was larger (i.e., the apparent vertex was closer to the GC-vertex) for the concave than convex angles, with an average difference of 8.5% (about 3 pixels). The amount of CCP effect measured with the probe localization technique was smaller than the corresponding 42% amount estimated from length-matching data obtained in Experiment 1. To explain this difference more empirical work is needed. However, notice that in the occluded condition of Experiment 1 observers were required to evaluate the interval between two partially-occluded convex shapes, while in Experiment 2 they were asked to explicitly attend to completion of the partially-occluded angle, in the attempt of accurately locating its vertex. Therefore, in Experiment 2 the distribution of attention might have favored the rectilinear extrapolation of T-stems and led to a smaller CCP effect. This interpretation is consistent with previous results showing that contour support ratio is effective only within the field of visual attention (Fantoni & Gerbino, 2002), and with the general assumption that effects of surface-level factors (in this case, minimal area) are more easily revealed when contour-level factors are weaker.

As regards the possible role of global surface properties, Experiment 2 did not support the hypothesis that the maximization of shape symmetry affects amodal completion in the direction of T-stem extrapolation. A possible influence of symmetry in the opposite direction, though suggested by data, seemed to us unlikely. We rather accounted for the pattern of IT penetrations in different conditions as a function of surface support ratio, a surface-level factor that appears to modulate the amount of CCP effect in a consistent manner. However, the major result of Experiment 2 was that the CCP effect is robust and survives important changes in the regularity and size of amodally-completed shapes.

11.1. Experiment 3: Plenum vs. vacuum

Results of Experiments 1 and 2 support the hypothesis that a tendency towards area minimization affects the shape of interpolated angles. Experiment 3 was designed to discriminate whether the minimal area hypothesis applies to the surrounded region or to the material surface. Such a test is possible given that the same surrounded region can be material or immaterial. A perceived hole represents the case of an immaterial region surrounded by a material surface. Irrespective of its shape, any region gains materiality as it becomes the surface closest to the viewpoint (Nakayama et al., 1989).

In Experiment 3 we used binocular disparity to specify depth in random dot stereograms. A butterfly region (derived from rotating the hourglass of Experiment 1) was defined by the correspondence of images shown to the two eyes. We compared the interpolation of the same closed contour in two conditions: when belonging to a material butterfly figure (crossed disparity) or to the surface surrounding an immaterial butterfly hole (uncrossed disparity). If area minimization applies to closed regions, irrespective of their materiality, interpolation trajectories should be the same in the two disparity conditions. Otherwise, if area minimization applies to material surfaces, interpolation trajectories should differ as a function of disparity.

As argued in Bertamini and Mosca (2004) random dot stereograms have specific advantages in the study of CCP. Firstly, fusion is necessary to perform the task, and therefore there is no ambiguity about what is seen as foreground and what is seen as background. Secondly, the surface occluding the target angles can be kept constant in different experimental conditions.

12. Method

12.1. Participants

Fifteen undergraduate students at the University of Liverpool participated in return for course credit. They all had normal or corrected vision and their ability to see stereograms was checked before the experiment started. Participants viewed all experimental displays (butterfly hole with comparison line in front, butterfly figure with comparison line in front, butterfly hole with comparison line on the background, butterfly figure with comparison line on the background).

12.2. Apparatus and displays

Stimuli were generated on a Macintosh G4 computer and presented on a Sony F500T9 monitor with a resolution of 1280×1024 pixels at 120 Hz. Two stereo images were presented with the use of a NuVision infrared emitter and stereoscopic glasses. The effect of interleaving left and right images was that effective vertical resolution and refresh rate were halved (512 pixels at 60 Hz). The computer recorded whether each response was correct and the reaction time in milliseconds using the VideoToolbox functions (Pelli, 1997).

A random-dot surrounding square ($18° \times 18°$ of visual angle) with zero disparity was always present on the screen. A random-dot butterfly (6° of visual angle wide) was presented as a figure when it was defined by crossed disparity (concave angle condition) or as a hole when it was defined by uncrossed disparity (convex angle condition). A black hexagonal occluder (3° of visual angle wide) with crossed disparity was present throughout the experiment (Fig. 11(a)). We saw no reason to define the occluder only by binocular disparity, and we opted for a black hexagon to make it as clear as possible that nothing was visible through it. The occluder was centered over the butterfly with orthogonal T-junctions. The horizontal separation between T-junctions was 20 pixels, the distance between the MP-line and the GC-vertex 10 pixels, the objective vertex separation 60 pixels, and contour support ratio 0.78. The center of the screen coincided with the center of the butterfly. Fig. 11(b) illustrates the stimulus in detail.

A red vertically-oriented line, 4-pixel thick, was displayed 3° from the left edge of the occluder. The line was displayed simultaneously with the stimulus. The observer controlled the line length by means of two keys on a game pad. Moreover, two locations in depth of the comparison line were used, to control for a possible role of the plane on which this line was located. The two depth locations corresponded to the plane of the butterfly figure (10′ crossed disparity) and to the plane of the surrounding square (zero disparity).

The target vertex separation was vertical (while it was horizontal in Experiment 1). We chose this orientation in Experiment 3 to make it orthogonal to binocular disparity.

12.3. Design and procedure

There were two within-subjects factors, CCP of target angles (concave for the material butterfly vs. convex for the material surround) and depth Location of the comparison line (front vs. back). They were factorially combined in a 2×2 design.

Participants were screened for stereoacuity using the TNO stereo test and for all of them the threshold was at worst 120″. Participants sat 58 cm from the screen in a quiet room under conditions of normal illumination. Each participant saw three practice trials, extracted at random from the experimental series of trials. After the practice the experimenter checked that the task was clear, and answered any questions. Next, the observers started the experimental session that consisted

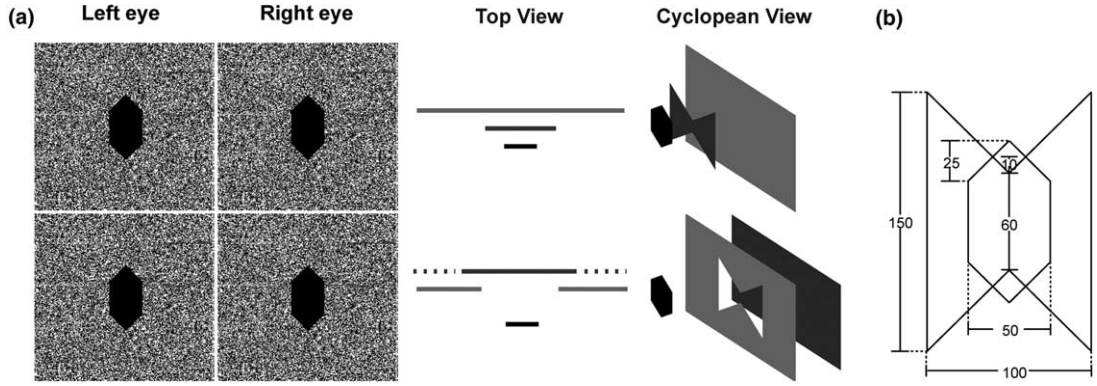

Fig. 11. (a) Random dot stereograms used in Experiment 3. When the upper two images are cross-fused a partially-occluded butterfly figure is perceived in front of the background plane, as shown in the top view (middle column) and in the simulation of the cyclopean view (right column). When the lower two images are cross-fused a partially-occluded butterfly hole is perceived. (b) Main stimulus linear extents in pixels.

of 12 trials (2 type × 2 line depth × 3 repetitions). It was stressed to the participants that there was no time pressure on their response, and they could make many adjustments in either direction until they were satisfied with their estimate.

Participants had to wear stereoscopic glasses throughout the experiment and were encouraged to take breaks if necessary. In Fig. 11(a), the left and the right images need to be fused to see an example of the stimuli. The reader can do this with the use of a stereo-viewer. Fig. 11(a) also provides the cyclopean views of hexagon-butterfly configurations.

Similarly to Experiment 1, the task can be described as having three stages: (i) the display was presented; (ii) the observer pressed one of two keys to adjust the length of the line; this stage could take a variable amount of time; (iii) after a 300-ms blank interval the next trial was presented.

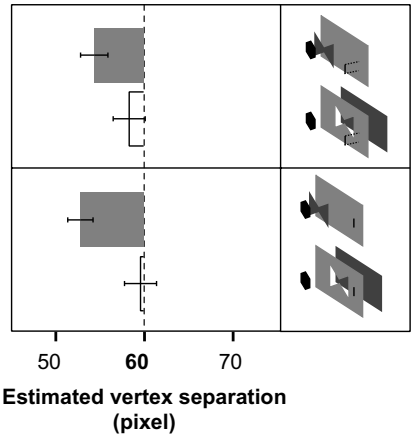

Fig. 12. Means and sem of estimated vertex separations as a function of CCP (grey = concave; white = convex) and of the depth location of the comparison line (upper two rows = front; lower two rows: back). Means are plotted as deviations from the objective vertex separation (60 pixels).

13. Results and discussion

We took the average of the three individual adjustments as the estimated vertex separation for every participant in each of the four conditions of the CCP x Location design. Estimated vertex separations of three participants, when transformed into z points, were lower than −1.96 (2.5%) or higher than 1.96 (97.5%) in at least one condition. Data from these participants were excluded from further analyses. In Fig. 12 means of estimated vertex separations (for the group of 12 participants) are plotted as deviations from the objective separation value (60 pixels).

Like in Experiment 1, statistical tests were performed after transforming the raw separation values into the signed square root of relative contrast percentages. Resulting means and sem were as follows: concave/back-line [0.03 ± 0.63]; concave/front-line [−0.38 ± 0.62]; convex/back-line [−2.17 ± 0.42]; convex/front-line [−1.68 ± 0.5].

We ran a within-subjects analysis of variance with CCP (concave vs. convex) and line Location (front vs. back) as factors. The CCP factor was significant ($F(1,11) = 12.14$, $p < 0.005$). The main effect of line Location ($F < 1$) and the interaction between CCP and Location ($F(1,11) = 2.95$) were not significant. Independent of the depth location of the probe, the mean vertical separation between vertices was more underestimated in the material butterfly condition (53.8 pixels) than in the material surround condition (59.0 pixels).

Pre-planned t-tests against the value of 60 confirmed a systematic tendency to underestimate the horizontal vertex separation in the figure condition [$t(24) = -5.23$, $p < 0.001$]. In contrast, the estimated vertex separation did not differ from the objective vertex separation in the hole condition [$t(24) = -0.66$, $p = 0.51$].

We found a CCP effect when participants estimated the separation of vertices of the same butterfly region,

depending on the figure-hole contrast. The effect is consistent with results of Experiments 1 and 2, and with the hypothesis that the area to be minimized is the one of the material surface. The difference between IT penetration values for convex angles (material surround) and concave angles (material butterfly) was 26% (2.6 pixels). This value is in between those of 42% penetration in Experiment 1 and 8.5% in Experiment 2.

14. General discussion

Our three experiments have shown that contour interpolation behind an occluder depends on contour curvature polarity, with greater extrapolation of contours of a partially-occluded concave angle with respect to the extrapolation of contours of the explementary convex angle. We used different global shapes, different luminance patterns, and different areas. In Experiment 3 surface materiality was manipulated by inverting binocular disparity. Under all conditions contour fragments belonging to a convex partially-occluded angle are extrapolated less than contour fragments belonging to the explementary concave partially-occluded angle.

As previously discussed, the effect of polarity on interpolated trajectories can be explained by a tendency to minimize the perceived area of material surfaces; what we refer to as the *minimal area hypothesis*. In Experiment 3 the polarity effect was obtained by shifting the ownership of the very same closed contour. This effect runs against an implication of the surprisal model by Feldman and Singh (2005). In fact, when applied to visual interpolation, the surprisal model generates different interpolated trajectories for closed contours with positive and negative curvatures, irrespective of the materiality of the bounded region.

No effect of global shape regularity (symmetry) was found in Experiment 2. Rather, data were consistent with the possible influence of surface support ratio, a surface-level factor that can be easily incorporated in the field model by Fantoni and Gerbino (2003). In such a model, good continuation and minimal path are conceived as context-sensitive unification principles. Interpolated trajectories result from chaining the sums of two vector fields, the GC-field and the MP-field. When contour fragments are rectilinear (like in present experiments) GC vectors are parallel to T-stems and their strength is an inverse function of distance from endpoints. On the other hand, MP vectors are parallel to the line joining the two endpoints and their strength is a direct function of distance from endpoints. Different values of GC–MP contrast (the relative strength of GC and MP maximal vectors) generate a family of interpolated trajectories, each corresponding to a smooth compromise between GC and MP solutions. Selection of a specific trajectory derives from the value of GC–MP contrast determined by contextual factors. We briefly describe here two modifications of the field model, which take into account the results of present experiments.

First, the architecture of the model is changed (Fig. 13) to include surface-level factors. Given the input image, two parallel streams of information are computed. Contour-level features such as position of T-junctions, orientation of T-stems, and lengths are processed in the *Contour stream*. Surface-based features such as shape regularity, area, and figure/ground assignment are processed in the *Surface stream*. The relative strength of GC- and MP-fields depends on the outputs of the two streams.

Second, area minimization (i.e., the principle we initially proposed to explain polarity effects) can be modeled as an effect of surface support ratio, the ratio between the areas of MP and GC completion solutions. This parameter enters the model as a weight—similar to contour support ratio—modulating the magnitude of the maximum GC vector. As the interpolation region bounded by GC extrapolation and the MP-line increases, surface support ratio departs from 1, linearly decreasing for the convex surface and linearly increasing for the concave surface. Consequently, the GC-field is weakened in the convex case and strengthened in the concave case. According to such an approach, the effect of contour curvature polarity derives from the modulating action of surface support ratio on GC–MP contrast.

Interestingly, as the amount of specified surface is increased, contour support ratio and surface support ratio cooperate in the convex condition, strengthening GC; while they act in opposite directions in the concave condition. In the latter case contour support ratio keeps its strengthening role, while surface support ratio acts as an attenuation factor.

Polarity effects are at odds with most current visual interpolation models, which are based entirely on contour-level information. As pointed out by Fantoni and Gerbino (2003, Table 1), such models represent a major attempt of providing precise interpolation solutions, but—contrary to empirical evidence—are invariant over contextual changes that affect contour curvature polarity and shape properties (size, orientation, regularity). The joining of fragment endpoints by invariant trajectories might be a desirable feature of an ideal observer, but does not fit human perception.

So far, the role of surface-level factors in visual interpolation has been overlooked. Non-geometric surface properties like color and texture (Yin, Kellman, & Shipley, 2000), as well as their interaction with geometric contour properties (Yin, Kellman, & Shipley, 1997), have been considered as determinants of the unification of image regions into perceptual wholes. Little attention has been devoted to the effects of geometric

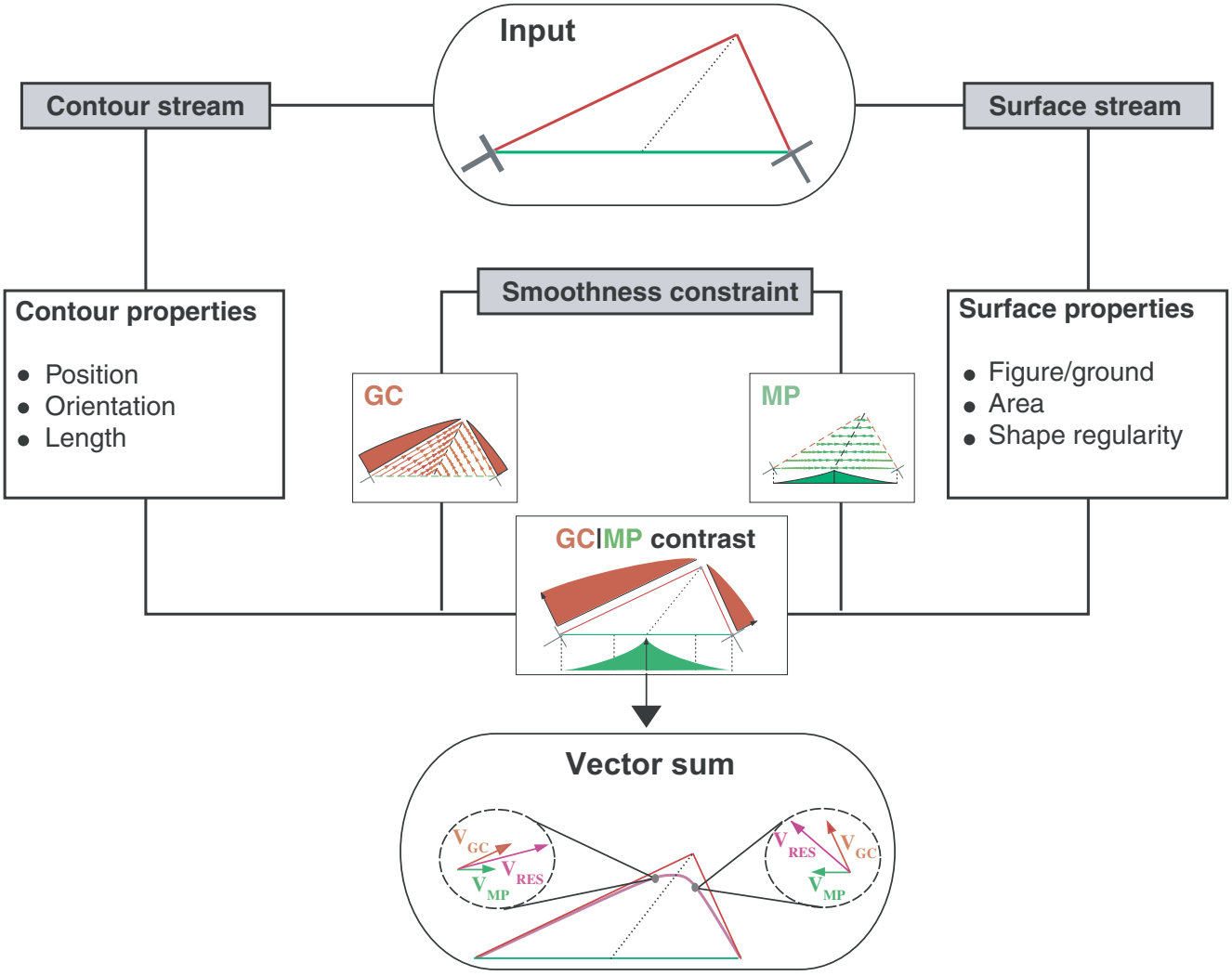

Fig. 13. The diagram illustrates the structure of the modified field model. The previous model (Fantoni and Gerbino, 2003) has been improved to account for both contour-level and surface-level determinants of visual interpolation.

surface-level factors on the precise shape of interpolated trajectories. Our findings are novel since they demonstrate that interpolation trajectories are affected by a fundamental geometric property of surface boundaries, contour curvature polarity. This calls for an update of current models of visual interpolation, including contour-based structural models (Guy & Medioni, 1996; Williams & Jacobs, 1997) and hybrid models in which a surface-completion process fills in the regions bounded by interpolated contours (Grossberg & Mingolla, 1985; Kellman, Guttman, & Wickens, 2001). The field model by Fantoni and Gerbino (2003) has been updated here.

More generally, although area minimization fits into the long-standing presence of the minimum principle in perception, it requires further study. In particular, we think that the relationship between surface support ratio and area minimization should be better understood, to cover a larger range of occlusion conditions.

Acknowledgements

The authors thank the editor and reviewers for criticism and suggestions. The revision has been completed during a visit of the first author at UCLA, where Philip Kellman provided him with an ideal environment for understanding the subtleties of visual interpolation. This work has been supported by a Miur-Cofin 2003 grant to Walter Gerbino.

References

Arnheim, R. (1954). *Art and visual perception: A psychology of the creative eye*. Regents of the University of California.

Asada, H., & Brady, M. (1984). The curvature primal sketch. Technical Report, MIT AI memo 758.

Attneave, F. (1954). Some informational aspects of visual perception. *Psychological Review, 61*, 183–193.

Baek, K., & Sajda, P. (2003). A probabilistic network model for integrating visual cues and inferring intermediate-level representa-

tions. In *Third international workshop on statistical and computational theories of vision* (SCTV'03), Nice, France.

Barenholtz, E., Cohen, E. H., Feldman, J., & Singh, M. (2003). Detection of change in shape: an advantage for concavities. *Cognition, 89*, 1–9.

Baylis, G. C., & Driver, J. (2001). Perception of symmetry and repetition within and across visual shapes: part-descriptions and object-based attention. *Visual Cognition, 8*, 163–196.

Bertamini, M., Friedenberg, J., & Argyle, L. (2002). No within-object advantage for detection of rotation. *Acta Psychologica, 111*, 59–81.

Bertamini, M. (2001). The importance of being convex: an advantage for convexity when judging position. *Perception, 30*, 1295–1310.

Bertamini, M., & Croucher, C. J. (2003). The shape of holes. *Cognition, 87*, 33–54.

Bertamini, M., & Mosca, F. (2004). Early computation of contour curvature and part structure: evidence from holes. *Perception, 33*, 35–48.

Boselie, F., & Leeuwenberg, E. (1986). A test of the minimum principle requires a perceptual coding system. *Perception, 15*, 331–354.

Fantoni, C., & Gerbino, W. (2002). Retinal size, visual attention, and contour interpolation. *Investigative Opthalmology & Visual Science, 4789*.

Fantoni, C., & Gerbino, W. (2003). Contour interpolation by vector-field combination. *Journal of Vision, 3*, 281–303, Available from http://journalofvision.org/3/4/4/, DOI 10.1167/3.4.4.

Feldman, J., & Singh, M. (2005). Information along contours and object boundaries. *Psychological Review*, *112*.

Finney, D. J. (1962). *Probit analysis* (2nd ed.). Cambridge, UK: Cambridge University Press.

Gerbino, W., & Fantoni, C. (2000). Amodal completion is not scale-invariant. *Investigative Opthalmology & Visual Science, 41*, S441, abstract 2335-B581.

Gerbino, W., & Fantoni, C. (2002). Contour polarity and visual interpolation. *Perception, 31*, Supplement.

Gerbino, W., Sgorbissa, F., & Fantoni, C. (2000). Good continuation and minimal path perturb symmetry judgments in amodal completion. *Abstracts of the Psychonomic Society, 5*.

Gibson, B. S. (1994). Visual attention and objects: one versus two or convex versus concave? *Journal of Experimental Psychology: Human Perception & Performance, 20*, 203–207.

Grossberg, S., & Mingolla, E. (1985). Neural dynamics of form perception: boundary completion, illusory figures, and neon color spreading. *Psychological Review, 92*, 173–211.

Guilford, J. P. (1963). *Psychometric methods*. New York: McGraw-Hill.

Guttman, S. E., & Kellman, P. J. (2004). Contour interpolation revealed by a dot localization paradigm. *Vision Research, 44*, 1799–1815.

Guy, G., & Medioni, G. (1996). Inferring global perceptual contours from local features. *International Journal of Computer Vision, 20*, 113–133.

Hoffman, D. D., & Richards, W. A. (1984). Parts of recognition. *Cognition, 18*, 65–96, [Also published as MIT AI Memo 732, 1983; In S. Pinker (Ed.), Visual cognition. MIT Press, 1985; In A. Pentland (Ed.), *From pixels to predicates: Recent advances in computational vision*, Ablex Publishing Company, 1986; and In M. Fischler & O. Firschein (Eds.), *Readings in computer vision*, Morgan & Kaufmann Publishers Inc., 1987.].

Hulleman, J., te Winkel, W., & Boselie, F. (2000). Concavities as basic features in visual search: evidence from search asymmetries. *Perception & Psychophysics, 62*, 162–174.

Humphreys, G. W., & Müller, H. (2000). A search asymmetry reversed by figure-ground assignment. *Psychological Science, 11*, 196–201.

Jacobs, D. W. (1996). Robust and efficient detection of salient convex groups. *IEEE Transactions on Pattern Analysis and Machine Intelligence, 18*, 23–37.

Kanizsa, G. (1979). *Organization in vision*. New York: Praeger.

Kanizsa, G., & Gerbino, W. (1976). Convexity and symmetry in figure-ground organization. In M. Henle (Ed.), *Vision and artifact* (pp. 25–32). New York: Springer Publishing Co.

Kellman, P. J., & Loukides, M. G. (1987). An object perception approach to static and kinetic subjective contours. In S. Petry & G. E. Meyer (Eds.), *The perception of illusory contours* (pp. 151–164). New York: Springer, Chapter 16.

Kellman, P. J., & Shipley, T. F. (1991). A theory of visual interpolation in object perception. *Cognitive Psychology, 23*, 141–221.

Kellman, P. J., Guttman, S. E., & Wickens, T. D. (2001). Geometric and neural models of object perception. In T. F. Shipley & P. J. Kellman (Eds.), *From fragments to objects: Segmentation and grouping in vision* (pp. 181–246). Amsterdam: Elsevier, Chapter 7.

Koenderink, J. (1984). What does the occluding contour tell us about solid shape?. *Perception, 13*, 321–330.

Koffka, K. (1935). *Principles of Gestalt psychology*. London: Routledge and Kegan.

Leeuwenberg, E. (1982). Metrical aspects of pattern and structural information theory. In J. Beck (Ed.), *Organization and representation in perception*. Hillsdale, NJ: Erlbaum.

Liu, Z., Jacobs, D. W., & Basri, R. (1999). The role of convexity in perceptual completion: beyond good continuation. *Vision Research, 39*, 4244–4257.

Massironi, M. (2002). *The psychology of graphic images: Seeing, drawing, communicating*. Hillsdale, NJ: Erlbaum.

Mumford, D. (1994). Elastica and computer vision. In C. Bajaj (Ed.), *Algebraic geometry and its applications* (pp. 491–506). New York: Springer-Verlag.

Nakayama, K., Shimojo, S., & Silverman, G. H. (1989). Stereoscopic depth: its relation to image segmentation, grouping, and the recognition of occluded objects. *Perception, 18*, 55–68.

Norman, J. F., Phillips, F., & Ross, H. E. (2001). Information concentration along the boundary contours of naturally shaped solid objects. *Perception, 30*, 1285–1294.

Pao, H.-K., Geiger, D., & Rubin, N. (1999). Measuring convexity for figure/ground separation. In *7th IEEE international conference on computer vision*, Kerkyra, Greece.

Pelli, D. G. (1997). The VideoToolbox software for visual psychophysics: transforming numbers into movies. *Spatial Vision, 10*, 437–442.

Preparata, F., & Shamos, I. (1985). *Computational geometry: An introduction* (2nd ed.). New York: Springer-Verlag.

Rubin, E. (1921). *Visuell wahrgenommene figuren*. Kobenhaven: Glydenalske boghandel.

Sekuler, A. B. (1994). Local and global minima in visual completion: effects of symmetry and orientation. *Perception, 23*, 529–545.

Shipley, T. F., & Kellman, P. J. (1992). Strength of visual interpolation depends on the ratio of physically specified to total edge length. *Perception & Psychophysics, 52*, 97–106.

Singh, M., & Hoffman, D. D. (2001). Part-based representations of visual shape and implications for visual cognition. In T. F. Shipley & P. J. Kellman (Eds.), *From fragments to objects: Segmentation and grouping in vision*. Amsterdam: Elsevier.

Takeichi, H. (1995). The effect of curvature on visual interpolation. *Perception, 24*, 1011–1020.

Takeichi, H., Nakazawa, H., Murakami, I., & Shimojo, S. (1995). The theory of the curvature-constraint line for amodal completion. *Perception, 24*, 373–389.

Ullman, S. (1976). Filling-in the gaps: the shape of subjective contours and a model for their generation. *Biological Cybernetics, 25*, 1–6.

van Lier, R., & Wagemans, J. (1999). From images to objects: global and local completions of self-occluded parts. *Journal of Experimental Psychology: Human Perception & Performance, 25*, 1721–1741.

van Lier, R., van der Helm, P., & Leeuwenberg, E. (1994). Integrating global and local aspects of visual occlusion. *Perception, 23*, 883–903.

Williams, L. R., & Jacobs, D. W. (1997). Stochastic completion fields: a neural model of illusory contour shape and salience. *Neural Computation, 9*, 837–859.

Xu, Y., & Singh, M. (2002). Early computation of part structure: evidence from visual search. *Perception & Psychophysics, 64*, 1039–1054.

Yin, C., Kellman, P. J., & Shipley, T. F. (1997). Surface completion complements boundary interpolation. *Perception, 26*, 1459–1479, [Special issue on surface appearance].

Yin, C., Kellman, P. J., & Shipley, T. F. (2000). Surface integration influences depth discrimination. *Vision Research, 40*, 1969–1978.

Zunic, J.D., & Rosin, P.L. (2002). A convexity measure for polygons. Paper presented at the British machine vision conference, Cardiff.